

Diving into a multi-band holographic superconductor

Xing-Kun Zhang,^a Xin Zhao,^a Zhang-Yu Nie,^c Ya-Peng Hu,^{a,b} Yu-Sen An.^{a,b,1}

^aCollege of Physics, Nanjing University of Aeronautics and Astronautics, Nanjing, 210016, China

^bMIIT Key Laboratory of Aerospace Information Materials and Physics, Nanjing University of Aeronautics and Astronautics, Nanjing, 210016, China

^cCenter for Gravitation and Astrophysics, Kunming University of Science and Technology, Kunming 650500, China

E-mail: anyusen@nuaa.edu.cn

ABSTRACT: In this paper, we consider the interior structure of a multi-band holographic superconductor model. We focus on the holographic superconductor system with two scalar fields which correspond to two s-wave order parameters in the dual condensed matter system. With two s-wave order parameters, the boundary system has more interesting behaviors which can also be reflected in black hole interior structure. We find the Einstein-Rosen bridge collapse and Josephson oscillations of two scalar fields inside the horizon. For the region near the singularity, we find that the metric still presents Kasner form and there is also Kasner transition behavior. However, when two scalar fields coexist, the Kasner exponents and Kasner transition formula will be different from the single scalar field case. The different interior structures between multi-band holographic superconductor and single-band holographic superconductor we find in this work further confirms that the black hole interior is important to reflect the properties of dual condensed matter systems.

¹Corresponding author.

Contents

1 Introduction:	1
2 Multi-band holographic superconductor with two scalar fields:	3
3 Interior structure of multi-band holographic superconductor:	6
3.1 General structures:	6
3.2 ER collapse and Josephson oscillation:	9
3.3 Kasner epoch:	11
3.4 Thermal a-function:	15
4 Conclusion and future direction	16
A More Kasner transition diagram:	17

1 Introduction:

AdS/CFT correspondence provides a useful tool to understand the strongly coupled condensed matter systems using dual gravitational framework [1, 2]. One prominent example is the holographic superconductor first raised in Ref.[3, 4] which is an s-wave superconductor model. The physical meaning of this holographic superconductor is as follows. From the bulk side, when gauge field and charged scalar fields are added, the original background without scalar hair (Reissner-Nordstrom black hole) will become unstable to form scalar hairs as we tune the temperature or chemical potential of the gravitational system. This spontaneously generated scalar hair can be understood as the order parameter of superconducting phase transition at the boundary by using AdS/CFT dictionary. Based on Ginzburg-Landau theory, this gravitational model mimics the superconducting phase transition. After the first discovery of this s-wave holographic superconductor model, there are many further generalizations to superconductor models with different types of order parameters, such as p-wave superconductor model [5, 6] and d-wave superconductor model [7, 8].

However, many realistic high T_c superconductor systems are characterized by multiple Fermi surfaces which means that there should be multiple order parameters in order to describe these systems [9, 10]. So many theoretical frameworks have also been established in condensed matter theory to understand multi-band superconductor models which have multiple order parameters [11, 12]. Holography provides a simple way to describe superconductors with multiple order parameters and many holographic models involving coexistence of multiple order parameters have been constructed. Ref.[13] builds a simple model to describe multi-band superconductor holographically. In this model, there are two charged

scalar fields coupled to the same $U(1)$ gauge field. It has been shown in Ref.[13] that there are cases where these two s-wave order parameters coexist. As this work was done in the probe limit, Ref.[14] generalized this result to fully back-reacted case and found that the coexistence region will enlarge when increasing the back-reaction. This multi-band model is $s + s$ type, there are also many further generalizations to the coexistence of $s + p$ order parameters [15], $p + p$ order parameters [16] and $s + d$ order parameters [17]. Ref.[18] gives a comprehensive review of the development of holographic superconductor model.

Above discussions regarding these holographic superconductor models only consider the black hole exterior region. This is because for the holographic study of condensed matter systems at finite temperature, the boundary state is a mixed state whose gravitational dual is the black hole exterior part. Thus it seems that black hole interior region is not related to these studies. However, the boundary mixed state can be purified to be a pure state. The most well-known purification is canonical purification and the resulting pure state is the thermo-field double state which reads

$$|TFD\rangle = \sum_i e^{-\beta E_i/2} |E_i\rangle_L |E_i\rangle_R \quad (1.1)$$

Once upon purification, the dual gravitational system of this pure state is the eternal AdS black hole (AdS wormhole) which contains the black hole interior part [19, 20]. For different systems with different Hamiltonians, the energy spectrum E_i will be different which leads to different properties of thermo-field double state. Certainly, this will also influence the interior structure of corresponding black holes and thus the features of black hole interior should also be important to illustrate the properties of boundary system.

Based on this consideration, many holographic investigations of boundary system have also been done from black hole interior point of view [21–38]. For holographic superconductor model, Ref. [22] investigated the interior structure of s-wave holographic superconductor proposed in [4]. They found that the black hole interior structure changes drastically after the superconducting phase transition. The original Cauchy horizon disappears due to the presence of scalar hair. And moreover, they also found a series of critical phenomena inside the horizon which are called "ER collapse" and "Josephson oscillation", these phenomena are most prominent near the critical temperature T_c . For the region near the singularity, there are also new behaviors. The metric takes the form of anisotropic Kasner universe and for unstable Kasner region, there also exists Kasner inversion behavior which follows the BKL transition rule [39]. It has also been found that different boundary models have different interior structures, for example the s-wave holographic superconductor model with exponential-type scalar potential and p-wave holographic superconductor model all bear distinct interior structures [26, 27, 29, 30]. Thus the black hole interior structures are very useful to characterize the distinct features of the boundary model.

Besides these progress, the investigations regarding the interior structure all focus on the single order parameter case. There is still no research on the interior structure of multi-band holographic superconductor model. From condensed matter point of view, the physics of multi-band superconductor will be very different from single-band superconductor, understanding this difference holographically is a very interesting question. As the black hole

interior structure can be a sensitive probe to the boundary model, thus we will investigate the interior structure of multi-band holographic superconductor in this paper. For simplicity, we will firstly focus on the multi-band holographic superconductor with two charged scalar fields. We find that with one additional scalar field, the Josephson oscillation behavior, Kasner geometry and Kasner transition behavior will all bear new features compared to single scalar field case.

The structure of this paper is as follows. In Sec.2, we first review the multi-band holographic superconductor with two competing scalar fields which have different mass and charge. We will show the three different types of coexistence behavior for different choice of parameters. In Sec.3, we will choose one specific coexistence scenario as a representative and investigate the interior structure of this hairy black hole with multiple scalar fields. We show the ER collapse, Josephson oscillation and Kasner behavior inside this black hole and describe its difference with the single scalar field case. In Sec.4, we conclude our paper and give some future directions.

2 Multi-band holographic superconductor with two scalar fields:

In this section, we will first give a brief introduction to the holographic multi-band superconductor model where two order parameters can coexist and compete. We will only focus on the case where two competing condensates are both scalar. To model the two s-wave orders on the boundary, we need to introduce two scalar fields in the bulk. Thus the action takes following form

$$S = \frac{1}{2\kappa^2} \int d^4x \sqrt{-g} [R + \frac{6}{L^2} - \frac{1}{4} F_{\mu\nu} F^{\mu\nu} + \sum_{k=1}^2 (-|\nabla\psi_k - ie_k A\psi_k|^2 - m_k^2 |\psi_k|^2)] \quad (2.1)$$

where the two scalar fields are minimally coupled to the same $U(1)$ gauge field and there is no direct interaction between them. e_k and m_k are the charge and mass of scalar field ψ_k , $\kappa^2 = 8\pi G$ is the Planck length and $F_{\mu\nu} = \nabla_\mu A_\nu - \nabla_\nu A_\mu$ is the electro-magnetic field strength.

Varying the action with respect to the metric field $g_{\mu\nu}$, electromagnetic field A_μ and scalar field ψ_k , we found the equation of motion reads,

$$D_{1\mu} D_1^\mu \psi_1 - m_1^2 \psi_1 = 0 \quad (2.2)$$

$$D_{2\mu} D_2^\mu \psi_2 - m_2^2 \psi_2 = 0 \quad (2.3)$$

$$\nabla^\mu F_{\mu\nu} = ie_1 [\psi_1^* D_{1\mu} \psi_1 - \psi_1 D_{1\mu}^* \psi_1^*] + ie_2 [\psi_2^* D_{2\mu} \psi_2 - \psi_2 D_{2\mu}^* \psi_2^*] \quad (2.4)$$

$$R_{\mu\nu} - \frac{1}{2} R g_{\mu\nu} - \frac{3}{L^2} g_{\mu\nu} = \frac{1}{2} F_{\mu\lambda} F_\nu^\lambda + \frac{1}{2} [(D_{1\mu} \psi_1 D_{1\nu}^* \psi_1^* + D_{2\mu} \psi_2 D_{2\nu}^* \psi_2^*) + \mu \leftrightarrow \nu] + \frac{g_{\mu\nu}}{2} L_m \quad (2.5)$$

where $L_m = -\frac{1}{4} F_{\mu\nu} F^{\mu\nu} - |D_1 \psi_1|^2 - m_1^2 |\psi_1|^2 - |D_2 \psi_2|^2 - m_2^2 |\psi_2|^2$ and we have defined $D_{1\mu} = \nabla_\mu - ie_1 A_\mu$, $D_{2\mu} = \nabla_\mu - ie_2 A_\mu$.

We consider the static and spherically symmetric metric ansatz

$$ds^2 = \frac{1}{z^2} (-f e^{-x} dt^2 + \frac{dz^2}{f} + dx^2 + dy^2) \quad (2.6)$$

and corresponding matter field ansatz

$$\psi_1 = \psi_1(z), \quad \psi_2 = \psi_2(z), \quad A = \phi(z)dt. \quad (2.7)$$

With these special ansatz, the equations of motion simplifies to

$$z^2 e^{\chi/2} (zh\psi_1')' = \frac{m_1^2 \psi_1}{z^2} - \frac{e^{\chi/2} e_1^2 \phi^2 \psi_1}{hz^3} \quad (2.8)$$

$$z^2 e^{\chi/2} (zh\psi_2')' = \frac{m_2^2 \psi_2}{z^2} - \frac{e^{\chi/2} e_2^2 \phi^2 \psi_2}{hz^3} \quad (2.9)$$

$$z^2 (e^{\chi/2} \phi')' = \frac{2\phi(e_1^2 \psi_1^2 + e_2^2 \psi_2^2)}{hz^3} \quad (2.10)$$

$$\chi' = z(\psi_1'^2 + \psi_2'^2) + \frac{\phi^2}{h^2 z^5} (e_1^2 \psi_1^2 + e_2^2 \psi_2^2) \quad (2.11)$$

$$4z^4 e^{\chi/2} h' = -12 + 2m_1^2 \psi_1^2 + 2m_2^2 \psi_2^2 + e^{\chi} z^4 \phi'^2 \quad (2.12)$$

where $h = \frac{f e^{-\chi/2}}{z^3}$ is introduced for convenience. The first two equations are scalar field equations and the third equation is Maxwell equation. The last two equations are two independent Einstein equations. Solving these five coupled differential equations with suitable boundary condition will holographically model the multi-band superconductor system. The parameter e_1, e_2 controls the back-reaction of the scalar field to the background. It has been found that the strength of backreaction will strongly influence the coexistence behavior of two scalar order parameter. To be more specific, increasing the backreaction (decreasing the charge) will enlarge the coexistence region[14].¹

For the convenience to perform numerics, we choose mass parameter of two scalar fields to be $m_1^2 = 0$ and $m_2^2 = -2$ respectively. For the spacetime having asymptotic AdS boundary, the general falloff of matter fields and metric fields near the boundary takes the form

$$\begin{aligned} \psi_1 &= \psi_1^{(0)} z^{\Delta_{1-}} + \psi_1^{(1)} z^{\Delta_{1+}} + \dots, & \psi_2 &= \psi_2^{(0)} z^{\Delta_{2-}} + \psi_2^{(1)} z^{\Delta_{2+}} + \dots \\ f &= \frac{1}{z^2} + \dots, & \chi &= 0 + \dots, & \phi &= \mu - \rho z + \dots \end{aligned} \quad (2.13)$$

By plugging these falloffs into the Klein-Gordon equation Eq.(2.8) and Eq.(2.9), mass-dimension relation in four dimension can be derived as

$$\Delta_1(\Delta_1 - 3) = m_1^2, \quad \Delta_2(\Delta_2 - 3) = m_2^2. \quad (2.14)$$

It can be easily solved that for the first scalar field, the conformal dimension is $\Delta_{1-} = 0$ and $\Delta_{1+} = 3$ and for the second scalar field, the conformal dimension is $\Delta_{2-} = 1$ and $\Delta_{2+} = 2$. Thus the expansion of scalar fields near boundary are correspondingly

$$\psi_1 = \psi_1^{(0)} + \psi_1^{(1)} z^3 + \dots, \quad (2.15)$$

$$\psi_2 = \psi_2^{(0)} z + \psi_2^{(1)} z^2 + \dots \quad (2.16)$$

¹Note that infinite charge limit corresponds to probe limit where back-reaction effect is switched off

We choose standard quantization procedure in this paper where $\psi^{(0)}$ is identified as the source and $\psi^{(1)}$ as the expectation value. To build a superconductor model, we require the scalar condensate is spontaneously generated thus we should set the boundary source term to be zero $\psi_{1,2}^{(0)} = 0$. By expanding the field near the horizon and plugging in the equations of motion, one finds that there are five independent parameters at the horizon $\{z_h, \psi_1(z_h), \psi_2(z_h), \phi'(z_h), \chi(z_h)\}$. Note that there are scaling symmetries associated to the equations of motion

$$e^{-x} \rightarrow \lambda^2 e^{-x}, \quad \phi \rightarrow \lambda \phi, \quad t \rightarrow \lambda^{-1} t; \quad (2.17)$$

$$z \rightarrow \lambda z, \quad (t, x, y) \rightarrow \lambda^{-1}(t, x, y), \quad f \rightarrow \lambda^2 f, \quad \phi \rightarrow \lambda \phi. \quad (2.18)$$

When performing numerics, we can first set $z_h = 1$ and $\chi(z_h) = 0$ and then use the first scaling symmetry to set $\chi(0) = 0$, this condition guarantees the asymptotic condition where the boundary time is the same as bulk time. Then we only have three independent parameters $\{\psi_1(z_h), \psi_2(z_h), \phi'(z_h)\}$, two of them will be chosen as shooting parameters to match the condition $\psi_{1,2}^{(0)} = 0$. Moreover for the expansion of electromagnetic field at boundary in Eq.(2.13), μ is the chemical potential and ρ is the charge density. We will work in grand canonical ensemble where the chemical potential should be kept fixed. By using the second scaling symmetry, we can set $\mu = 1$ at the boundary to achieve this.

At high temperature, the normal phase is dominant which is RN-AdS black hole where two scalar field vanishes $\psi_1 = \psi_2 = 0$. After decreasing temperature, the spontaneous symmetry breaking happens and scalar order parameter appears. It is interesting to note that when there are two scalar fields, when further lowering the temperature, second order parameter will appear which have significant influence on the first order parameter. Most notably, it was plotted in Fig.1 that second order parameter will suppress the first order parameter² and by further decreasing temperature, the second order parameter will still increase and the first order parameter will decrease to zero. This case is called phase-X in Ref.[14]. In this case, the two order parameters have strong competition between each other. The competition can also be seen in black hole exterior configuration shown in Fig.2. Furthermore, by increasing the backreaction (decreasing the parameter e_1 or e_2), it was found in Ref.[14] that strong backreaction will enlarge the coexistence region which makes two order parameters always coexist. Ref.[14] found two possible phases, one is shown in the left panel of Fig.3 for the parameter $e_2 = 2$ and $e_1/e_2 = 1.95$ which is called phase-A in [14], and another is shown in the right panel of Fig.3 for the parameter choice $e_2 = 1.5$ and $e_1/e_2 = 1.9$ which is called phase-B in [14].

These condensate behaviors imply that the microscopic physics behind this superconductor model will be much more complex than the single order parameter case. It is natural to expect that this complicated boundary physical structure can also be reflected in terms of black hole interior. Thus in the next section, we will investigate this physical behavior from the black hole interior point of view.

²Note that we rescale the condensate value using e_2 in this figure to match the notation in Ref.[14].

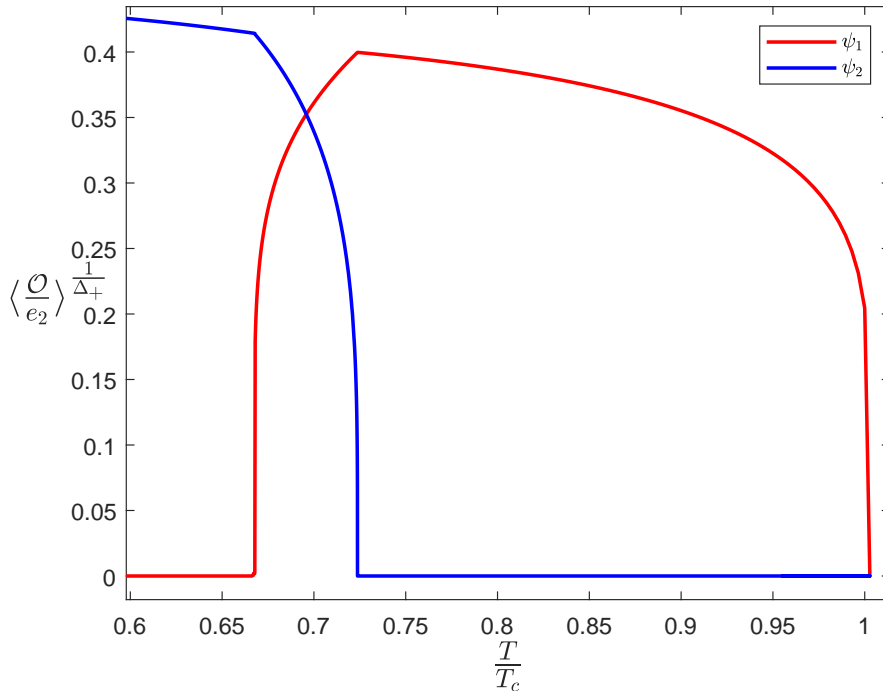


Figure 1. Phase X of multiple order parameters in holographic superconductor. This figure is plotted for parameter $e_2 = 4$ and $e_1/e_2 = 1.95$. The red curve corresponds to ψ_1 while the blue curve corresponds to ψ_2 . We fix chemical potential $\mu = 1$ in this figure. It can be seen that when the second order parameter appears, it suppresses the first order parameter

3 Interior structure of multi-band holographic superconductor:

In this section, we will investigate the interior structure of multi-band holographic superconductor. We only investigate these phenomena in Phase-X case, behaviors in Phase-A and Phase-B case are similar.

3.1 General structures:

For charged black hole with scalar hair, it can be shown that when the scalar hair forms, no matter how small it is, it can induce strong non-linear effect which removes the Cauchy horizon [21, 22, 24]. There are many proofs of the no Cauchy horizon theorem by using conserved charge method and energy condition method [21, 24, 40]. We only briefly introduce the conserved charge method here. As the model has scaling symmetry, there is a conserved charge associated to this symmetry by Noether theorem. The conserved charge reads

$$Q(z) = e^{\chi/2} [z^{-2} (f e^{-\chi})' - \phi \phi']. \quad (3.1)$$

It can be directly verified that $Q'(z) = 0$ by using the equation of motion from Eq.(2.10) to Eq.(2.12). Assuming the black hole has two horizons at z_h and z_i , thus the blackening

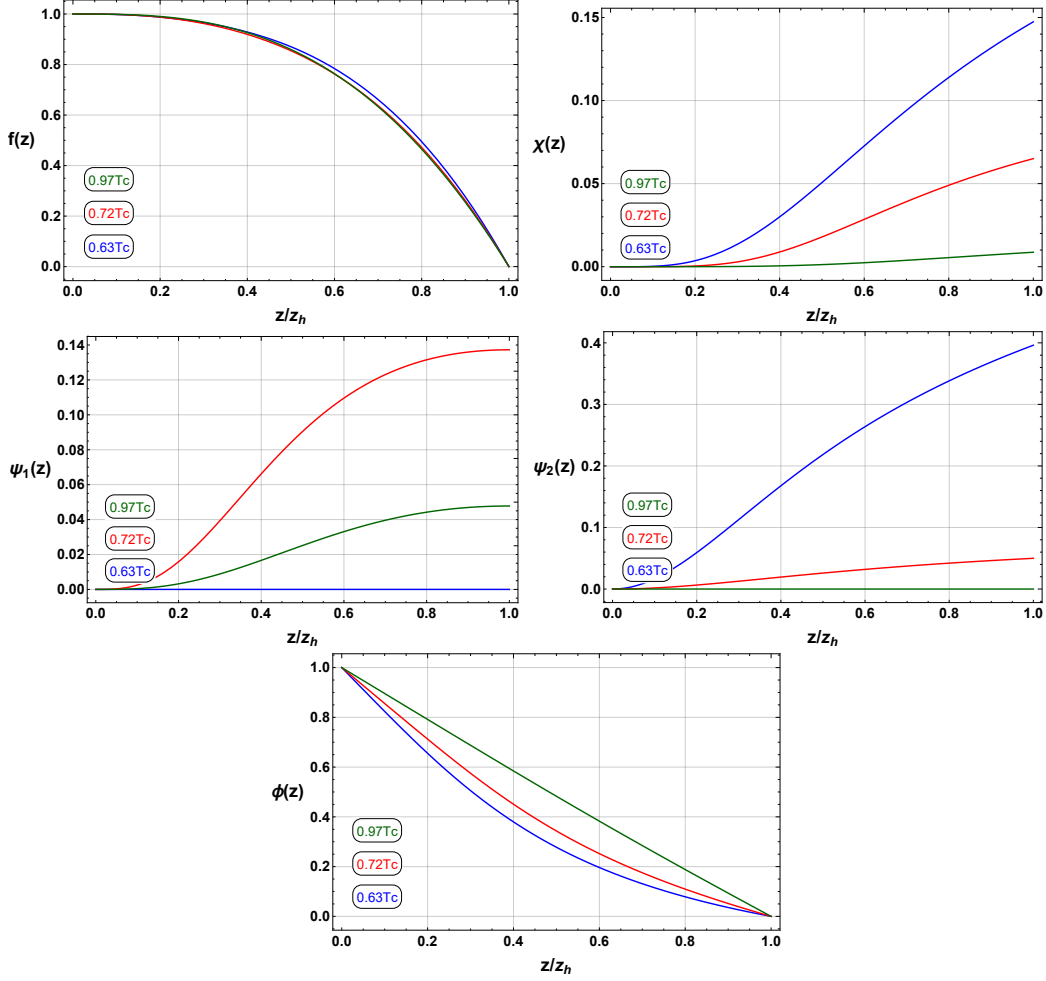


Figure 2. The configuration of charge black holes with scalar hair from the event horizon, $z = z_H$, to the AdS boundary, $z = 0$, at different temperatures. We have fixed the chemical potential $\mu = 1$.

factor $f(z)$ will satisfy the condition

$$\begin{aligned} f(z_h) &= 0, & f'(z_h) &< 0, \\ f(z_i) &= 0, & f'(z_i) &> 0. \end{aligned} \quad (3.2)$$

There are also constraints on the gauge field by the regularity of equation of motion

$$\phi(z_h) = \phi(z_i) = 0 \quad (3.3)$$

By using the conditions (3.2) and (3.3), we can find

$$Q(z_h) = Q(z_i) \rightarrow \frac{f'(z_h)}{z_h^2} e^{-\chi(z_h)/2} = \frac{f'(z_i)}{z_i^2} e^{-\chi(z_i)/2} \quad (3.4)$$

This can not be true as the blackening factor must obey Eq.(3.2) as there are two horizons. Thus the assumption that the black hole has two horizons is wrong and there is only

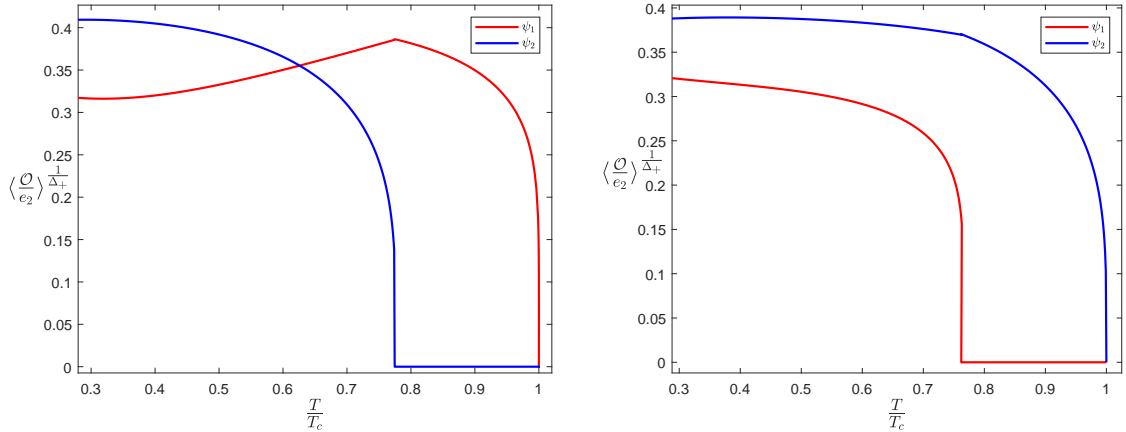


Figure 3. Multiple order parameters in holographic superconductor for larger backreaction. **Left panel:** Phase A with $e_2 = 2$ and $e_1/e_2 = 1.95$. **Right panel:** Phase B with $e_2 = 1.5$ and $e_1/e_2 = 1.9$. The red curve corresponds to ψ_1 while the blue curve corresponds to ψ_2 . We fix chemical potential $\mu = 1$ in this figure. It can be seen that by increasing the backreaction, the suppressive effect of second order parameter will be less dramatic and the two order will always coexist.

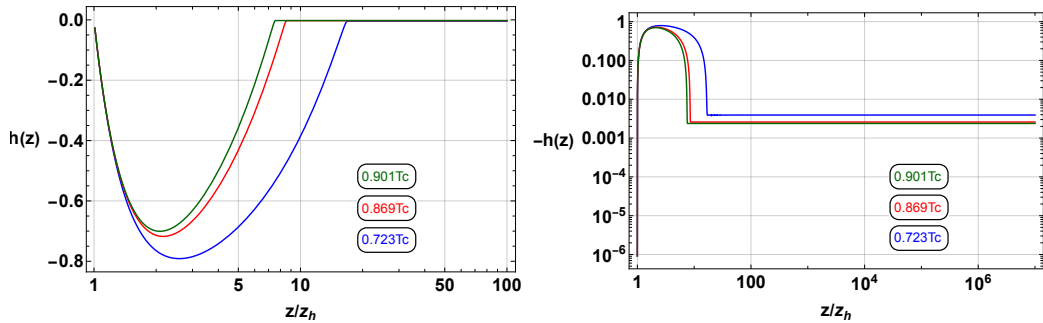


Figure 4. **Left panel:** Metric function $h(z)$ inside black hole for the region not far from horizon. **Right panel:** Metric function $-h(z)$ inside black hole for the region far from horizon. We see $h(z)$ is an $O(1)$ quantity in the deep interior which means the singularity is space-like.

one horizon for black hole with scalar hair³. Note that this proof is valid for arbitrary numbers of minimally coupled scalar fields, thus there is no Cauchy horizon in our multi-band superconductor model and the black hole singularity becomes space-like when scalar charge forms. Absence of Cauchy horizon can also be corroborated by the numerical result, we plot the spacetime interior structure and gauge field behavior inside black hole in Fig.4 and Fig.5 to show this. It is easy to see that $h(z) = 0$ and $\phi(z) = 0$ have only one root which means the black hole has only one horizon.

³This proof is also valid for $k = +1$ case, however we only focus on $k = 0$ case in our paper as our holographic superconductor is in $k = 0$ case

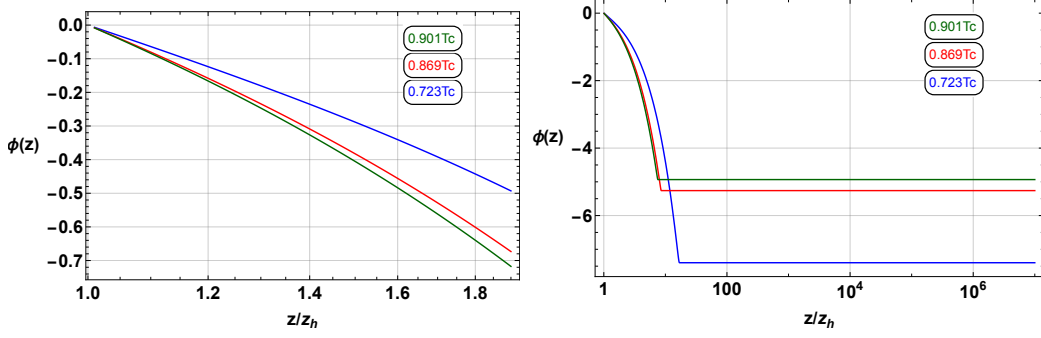


Figure 5. Gauge field $\phi(z)$ inside black hole. **Left panel:** not so far from horizon. **Right panel:** deep inside horizon.

3.2 ER collapse and Josephson oscillation:

Besides the absence of Cauchy horizon, there are also more novel behaviors inside the corresponding scalar hairy black hole. In this section, we will investigate the ER collapse and Josephson oscillation behavior. Near the horizon, there will be sudden decrease of metric function g_{tt} which is so called ER collapse [23]. This rapid collapse of g_{tt} is a critical phenomenon which is only notable near the critical temperature T_c . We plot the ER collapse behavior in different temperature in Fig.6. It can be seen here that the ER collapse will be less dramatic as we lower the temperature away from T_c . ER collapse is closely related to

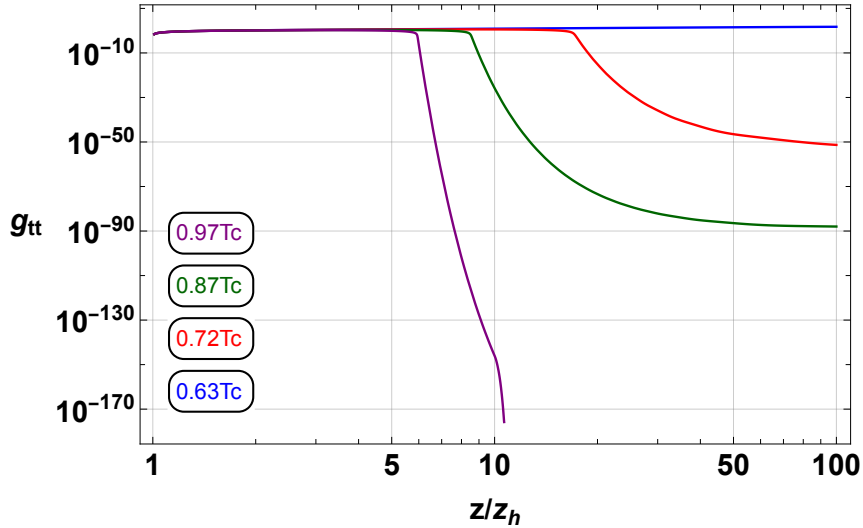


Figure 6. ER collapse behavior inside the holographic superconductor, we see that the ER collapse is less dramatic as we lower the temperature away from critical temperature

the phenomenon called Josephson oscillation. The scalar field inside black hole can have oscillations right after ER collapse happens. This can be found in terms of the equation of

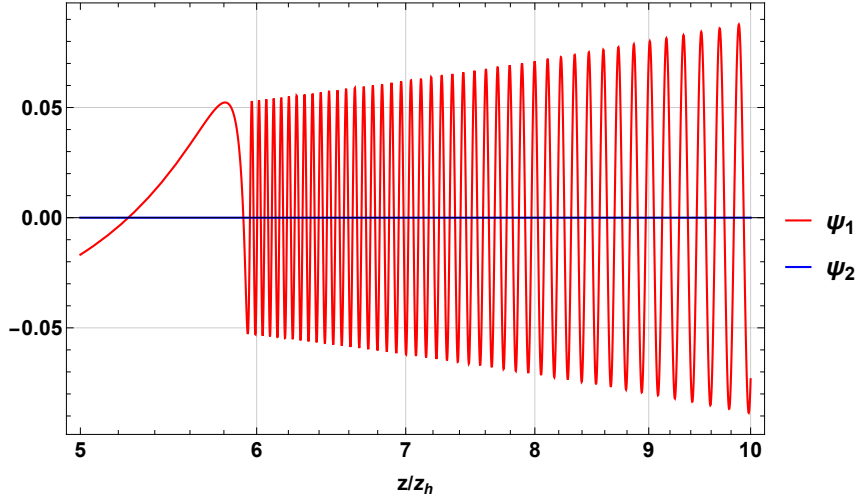


Figure 7. Scalar oscillation behavior for $T = 0.97T_c$, at this temperature the second scalar field ψ_2 has not appeared and the ψ_1 field rapidly oscillate.

motion of scalar field ⁴ which reads

$$\psi'' + \frac{h'}{h}\psi' + \frac{\psi'}{z} = -\frac{q^2\phi^2\psi}{z^6h^2} + \frac{m^2\psi}{z^5h}e^{-\chi/2} \quad (3.5)$$

After ER collapse, $e^{-\chi/2}$ is vastly small thus the mass term and h'/h term can be neglected. Moreover, it can be checked numerically in Fig.4 and Fig.5 that the ϕ^2/h^2 term is approximately a constant after ER collapse. After using these approximations, the scalar field can be solved as

$$\psi = c_J J_0\left(\frac{\phi}{2hz^2}\right) + c_Y Y_0\left(\frac{\phi}{2hz^2}\right) \quad (3.6)$$

where c_J, c_Y are two integration constants and J_0, Y_0 are first kind and second kind Bessel function respectively. Eq.(3.6) is a highly oscillating function which is denoted as "Josephson oscillation" in Ref.[22] to show its connection to Josephson effect in superconductor.

This analytical argument can also be corroborated by the numerical result. We plot the Josephson oscillation behavior of holographic multi-band superconductor in Fig.7 and Fig.8. For the temperature close to the critical temperature, we see that there is one scalar hair and as ER collapse is dramatic, the scalar field rapidly oscillates as shown in Fig.7. As we lower the temperature, two things happen. Firstly, the ER collapse becomes less dramatic which leads to slower oscillation of scalar field. Secondly, below a certain temperature ($T = 0.72360T_c$ in our case), second scalar field will appear. As we show in Fig.1, for temperature $T = 0.72T_c$, the temperature lies in the domain where there are two coexisted scalar fields. At this temperature, since the ER collapse is still not negligible, two scalar oscillations will appear as shown in the left panel of Fig.8. When further lowering the temperature, the ER collapse and Josephson oscillation cease to exist which is shown in the right panel of Fig.8.

⁴The two scalar fields have the same form of equation of motion, ψ here denotes either ψ_1 or ψ_2

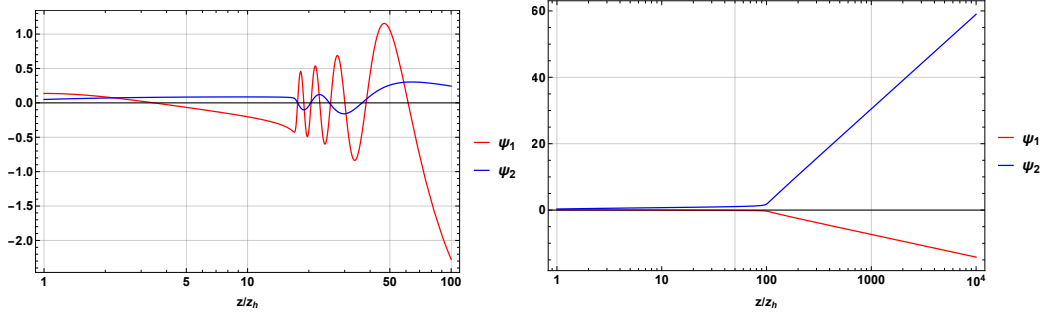


Figure 8. Scalar oscillation behavior for $T = 0.72T_c$ and $T = 0.68T_c$. For $T = 0.72T_c$ case, the ψ_1, ψ_2 coexist and oscillate. After further lowering the temperature, the oscillation disappears as a result of the lack of ER collapse.

3.3 Kasner epoch:

In the last section, we focus on the black hole interior structure near the horizon r_h . From the behavior of $z\psi'$ in Fig. 9, we see that $z\psi'_{1,2}$ approach constants in the deeper interior. This behavior will indicate that the system enters into the Kasner epoch, thus in this section

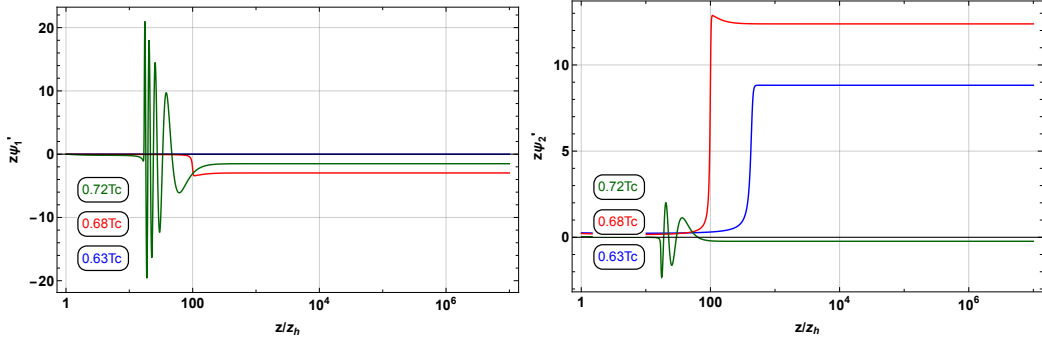


Figure 9. The scalar field behavior inside black hole. **Left panel:** we plot the behavior of $z\psi'_1$. **Right panel:** we plot the behavior of $z\psi'_2$. $z\psi'$ approaches constant in the deep interior implies that the metric enters into the Kasner epoch.

we will turn to investigate the black hole interior structure in this deep region for multi-band case. We can check numerically that in this region, the mass term and charge term in the equations of motion can be neglected, and the equation of motion for ψ_1, ψ_2 and χ can be vastly simplified as follows

$$\psi_1'' \approx -\frac{1}{z}\psi_1', \quad \psi_2'' \approx -\frac{1}{z}\psi_2', \quad \chi' \approx z(\psi_1'^2 + \psi_2'^2). \quad (3.7)$$

After this approximation, the scalar field could be solved as

$$\psi_1 \sim \alpha_1 \ln z, \quad \psi_2 \sim \alpha_2 \ln z \quad (3.8)$$

for region near the singularity $z \rightarrow \infty$, where α_1, α_2 are two constants. The function χ can also be directly calculated as

$$\chi \sim (\alpha_1^2 + \alpha_2^2) \ln z \quad (3.9)$$

As can be verified from numerical results in Fig.4 posteriorly, $h = \frac{fe^{-\chi/2}}{z^3}$ is a $\mathcal{O}(1)$ quantity, thus we found

$$f \sim z^{3+\frac{1}{2}\alpha_1^2+\frac{1}{2}\alpha_2^2} \quad (3.10)$$

By using the metric ansatz in Eq.(2.6) the metric component g_{zz} at large z reads

$$g_{zz} \sim \frac{1}{z^{5+\frac{1}{2}\alpha_1^2+\frac{1}{2}\alpha_2^2}} \quad (3.11)$$

By transforming to proper time τ using the relation

$$d\tau = \frac{dz}{z^{\frac{5}{2}+\frac{\alpha_1^2}{4}+\frac{\alpha_2^2}{4}}} \quad (3.12)$$

we found that

$$z \sim \tau^{-\frac{1}{\frac{3}{2}+\frac{1}{4}\alpha_1^2+\frac{1}{4}\alpha_2^2}} \quad (3.13)$$

Thus the metric near the singularity reads

$$ds^2 = -d\tau^2 + \tau^{2p_t} dt^2 + \tau^{2p_x} dx^2 + \tau^{2p_y} dy^2 \quad (3.14)$$

with Kasner exponent $p_t = \frac{\alpha_1^2+\alpha_2^2-2}{\alpha_1^2+\alpha_2^2+6}$ and $p_x = p_y = \frac{4}{\alpha_1^2+\alpha_2^2+6}$, it can be easily checked that Kasner exponents satisfy the relation

$$p_t + p_x + p_y = 1 \quad (3.15)$$

Also we can define p_ψ as $\psi \sim -p_\psi \ln \tau$ and find that

$$p_{\psi_1} = \frac{4\alpha_1}{\alpha_1^2 + \alpha_2^2 + 6}, \quad p_{\psi_2} = \frac{4\alpha_2}{\alpha_1^2 + \alpha_2^2 + 6} \quad (3.16)$$

Thus we find another relation among Kasner exponents,

$$p_t^2 + p_x^2 + p_y^2 + p_{\psi_1}^2 + p_{\psi_2}^2 = 1. \quad (3.17)$$

In this Kasner regime, the Maxwell equation can also be easily solved, where the electromagnetic field reads

$$\phi \sim \phi_0 + E_0 z^{1-\frac{1}{2}\alpha_1^2-\frac{1}{2}\alpha_2^2} \quad (3.18)$$

with ϕ_0 and E_0 two integration constants. It can be seen that for $\alpha_1^2 + \alpha_2^2 < 2$, the electromagnetic field will grow for large z . Thus for the case $\alpha_1^2 + \alpha_2^2 < 2$, the accumulated electro-magnetic field can become important which makes the Kasner region unstable. The unstable Kasner region will transit to another stable Kasner region. So in the following, we should take this fact into account and investigate the Kasner transition behaviors for multi-band holographic superconductor.

In the Kasner region, as verified posteriorly that the term involving e_1 and e_2 and m in all the equations of motion can be neglected. The Maxwell equation and Einstein equation involving h can be solved as

$$\phi = \phi_0 + E_0 \int e^{-\chi/2} dz \quad (3.19)$$

$$h = \frac{E_0^2}{4} \int e^{-\chi/2} dz - \frac{1}{c} \quad (3.20)$$

where ϕ_0, E_0 and c are three integration constants. Moreover, by re-writing scalar field as

$$\psi_1 = \int \frac{\alpha_1(z)}{z} dz, \quad \psi_2 = \int \frac{\alpha_2(z)}{z} dz \quad (3.21)$$

the equation of χ in Eq.(3.7) becomes

$$\chi' = \frac{\alpha_1(z)^2 + \alpha_2(z)^2}{z} \quad (3.22)$$

Plugging Eq.(3.20-3.22) into the scalar field equations, the scalar field equations become

$$\alpha_2^2 + \alpha_1^2 + 2z \frac{\alpha_1''}{\alpha_1'} - 4z \frac{\alpha_1'}{\alpha_1} = 0 \quad (3.23)$$

$$\alpha_1^2 + \alpha_2^2 + 2z \frac{\alpha_2''}{\alpha_2'} - 4z \frac{\alpha_2'}{\alpha_2} = 0 \quad (3.24)$$

Note that when one of the scalar fields vanishes, the above differential equations becomes one single equation

$$\alpha^2 + 2z \frac{\alpha''}{\alpha'} - 4z \frac{\alpha'}{\alpha} = 0 \quad (3.25)$$

which can be directed solved as

$$(\alpha - \alpha_0)^{-2/(2-\alpha_0^2)} \left(\frac{2}{\alpha_0} - \alpha \right)^{-1/(1-2/\alpha_0^2)} \alpha = \frac{z_{in}}{z} \quad (3.26)$$

where z_{in} is an integration constant. This solution tells us that if the first Kasner epoch has the feature $\alpha_0 < \sqrt{2}$, when increasing z , $\alpha(z)$ should transit from α_0 to $2/\alpha_0$. This is the so called "Kasner inversion" behavior which is first introduced in Ref. [22].⁵ However, the presence of second scalar field will change this inversion behavior, the second scalar field will make the differential equation become the coupled differential equations. The differential equations Eq.(3.23)and Eq.(3.24) may not be directly solved analytically, but in all the cases where Kasner transition happens, we can find numerically that the Kasner transition has two interesting relations

$$\alpha_1 \beta_1 + \alpha_2 \beta_2 = 2, \quad \alpha_1 \beta_2 = \alpha_2 \beta_1 \quad (3.27)$$

where α_1 and β_1 are the values of $z\psi_1'$ before and after transition, and α_2 and β_2 are the values of $z\psi_2'$ before and after transition. We show one example of this Kasner transition behavior in Fig.10, and more cases are presented in appendix A in Fig.12. The results are also summarized in the Table 1 .

It is interesting to check that these two conditions are crucial to make the Kasner transition follow the BKL transition rule [39, 42] which is

$$p_t \rightarrow -\frac{p_t}{2p_t + 1}, \quad p_x \rightarrow \frac{p_x + 2p_t}{2p_t + 1}, \quad p_y \rightarrow \frac{p_y + 2p_t}{2p_t + 1} \quad (3.28)$$

⁵The Kasner transition behaviors are different for different matter fields or gravitational theories, for more discussions see Ref.[27, 30, 38, 41].

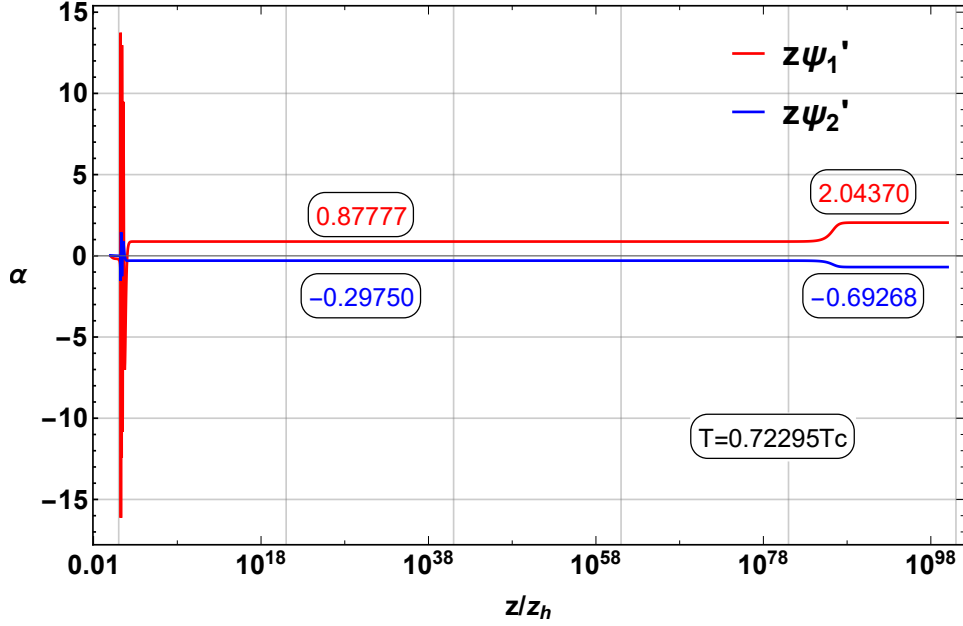


Figure 10. Kasner transition behavior for $T = 0.72295T_c$. We find that the exponents before and after the transition satisfy the relation in Eq.(3.27)

T/T_c	α_1	α_2	β_1	β_2	$\alpha_1\beta_1 + \alpha_2\beta_2$	$\alpha_1\beta_2 - \alpha_2\beta_1$
0.72295	0.87777	-0.29750	2.04370	-0.69268	1.99997	5×10^{-5}
0.72292	0.71784	-0.29806	2.37641	-0.98672	1.99998	2×10^{-5}
0.72275	-0.09648	-0.28950	-2.07215	-6.21778	1.99997	2×10^{-5}
0.72265	-0.58321	-0.27603	-2.80165	-1.32601	1.99997	2×10^{-6}
0.72261	-0.74294	-0.27026	-2.37738	-0.86482	1.99998	1×10^{-6}

Table 1. The exponents before and after the Kasner transition calculated by numerics. It can be found that the relation in Eq.(3.27) holds in all cases.

We see that p_t changes signs during the transition period. Before the transition, p_t is negative as a result of $\alpha_1^2 + \alpha_2^2 < 2$ while p_t is positive after the transition. Therefore, $p_t < 0$ which physically means that spatial t direction of the geometry expands is an unstable period while $p_t > 0$ is a stable period. As proved in Ref.[43], as long as scalar fields are minimally coupled, there is final Kasner regime no matter how many scalar fields are. So there will be no more Kasner transition after entering into $p_t > 0$ region.

Moreover, Kasner exponents p_t and p_x are also sensitive to the temperature. We plot the relation between the final Kasner exponents and temperature in Fig. 11. We find that Kasner exponents p_t and p_x have irregular behavior in terms of temperature. Furthermore, we also compare the Kasner exponents in multiple order parameters case with the Kasner exponents in single order parameter case. We find that when the second order parameter appears below $T = 0.72360T_c$, the Kasner exponents will be significantly shifted which means that Kasner exponents near the singularity are sensitive probes of the phases of boundary condensed matter system.

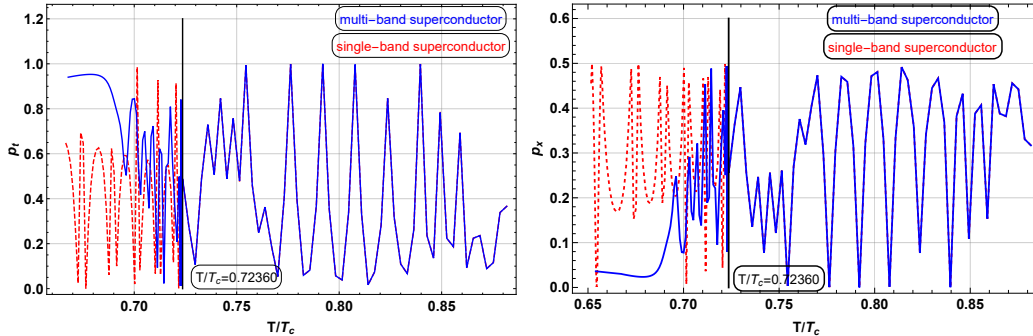


Figure 11. The Kasner exponents in multi-band superconductor are plotted in blue solid line, from which we see Kasner exponents p_t and p_x depend sensitively on the temperature. We also plot the Kasner exponents of single band superconductor (with only ψ_1 field) using red dotted line for comparison. We find that the additional order parameter ψ_2 will significantly alter the Kasner exponent.

3.4 Thermal a-function:

The difference between Kasner exponents we found in Fig.11 can also be reflected in other physical quantities. In this section, we choose the thermal a-function which was originally raised in [44] to illustrate this.

For AdS black hole, the radial coordinate z is commonly treated as an energy scale which parameterized the renormalization group flow from the UV CFT on the boundary to the IR CFT on the horizon. It was shown in [44] that by analytically continuation, the holographic renormalization group flow can also be generalized to describe the black hole interior region, which is called trans-IR flow. Along the flow from UV to IR and then to trans-IR region, a monotonic function can be defined which is called thermal a-function in [44]. The thermal a-function measures the effective number of degrees of freedom for each energy scale along the RG flow whose expression in $d + 1$ dimensions is

$$a_T(u) = \frac{\pi^{d/2}}{\Gamma(\frac{d}{2})\kappa^{d-1}} \left(\frac{\sqrt{f(u)}e^{-\chi/2}}{A'(u)} \right)^{d-1} \quad (3.29)$$

where κ is the Planck length and

$$\frac{du}{dz} = -\frac{1}{z\sqrt{f}}, \quad e^{2A(u)} = \frac{1}{z^2}. \quad (3.30)$$

Moreover, the thermal a-function can be proved to be monotonically decreasing by using null energy condition.

We choose to still use the coordinate in Eq.(2.6) to express the thermal a-function. In four dimensional case, the thermal a-function simplifies to be

$$a_T(z) = \frac{2\pi}{\kappa^2} e^{-\chi}. \quad (3.31)$$

Note that the monotonically decreasing behavior of thermal a-function can also be seen from the monotonically increasing behavior of χ field. Near the singularity, we found that

the thermal a-function becomes

$$a_T(z)|_{kasner} = \frac{2\pi}{\kappa^2} e^{-(\alpha_1^2 + \alpha_2^2) \ln z} = \frac{2\pi}{\kappa^2} z^{-\frac{6p_t+2}{1-p_t}} \quad (3.32)$$

where we use Eq.(3.9). Thus we see that the thermal a-function in Kasner region is solely determined by the Kasner exponent p_t and different behavior of Kasner exponent will lead to different behavior of thermal a-function (or different behavior of effective degrees of freedom). So the thermal a-function is a good physical quantity to reflect the different interior structure between multi-band superconductor model and single band superconductor model.

4 Conclusion and future direction

In this work, we investigate the interior structure of holographic multi-band superconductor. Besides the boundary phase diagram, the black hole interior structures are also modified by the additional scalar field. There is ER collapse epoch after which Josephson oscillation occurs. When lowering the temperature below which second scalar condensate appears, there will be oscillation behavior of two scalar fields. Moreover, the additional scalar field also has contributions to the Kasner exponent which makes the Kasner exponent different from the single scalar case. The Kasner transition behavior will also be more complicated in double scalar case, which presents more complex relations compared to the "Kasner inversion" phenomenon in single scalar case. Finally, we show that the difference between the Kasner exponent p_t can also be reflected in the thermal a-function. These results show that the difference between boundary field theory systems can be reflected in terms of black hole interior structure especially the structure near the black hole singularity.

There are several interesting directions to be pursued in the future investigations. Firstly, we only investigate the multi-band holographic superconductor model for two s-wave order parameters case. As p-wave superconductor has more intricate interior structure compared with s-wave case [26]. Thus it is also interesting to investigate the interior of multi-band model with coexistence of s-wave and p-wave order parameters [15]. Moreover, besides thermal a-function, there are also proposals using correlation functions [45–47] and complexity [48] to characterize the information of black hole interior (especially the information near the singularity), it is also intriguing to see the behaviors of these variables in holographic multi-band superconductor model.

Acknowledgments

We are grateful for the useful discussions with our group members. This work is supported by the National Natural Science Foundation of China (NSFC) under Grant Nos.12405066, 12175105 and 11965013. YSA is also supported by the Natural Science Foundation of Jiangsu Province under Grant No. BK20241376.

A More Kasner transition diagram:

In this appendix, we show more examples where the Kasner epochs have transition behavior in Fig.12, these transition behaviors all satisfy the relation we found in Eq.(3.27) thus obeying BKL transition relation.

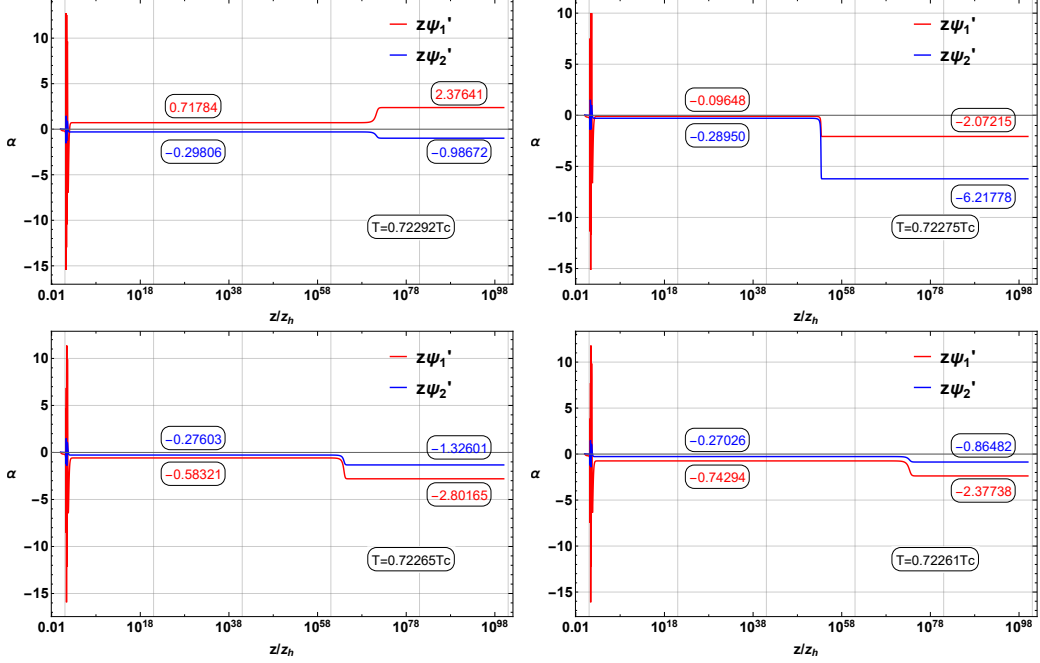


Figure 12. Kasner inversion behavior for $T = 0.72292T_c$, $T = 0.72275T_c$, $T = 0.72265T_c$ and $T = 0.72261T_c$, all of these example satisfy the two relations in Eq.(3.27)

References

- [1] Juan Martin Maldacena. The Large N limit of superconformal field theories and supergravity. *Adv. Theor. Math. Phys.*, 2:231–252, 1998.
- [2] Ofer Aharony, Steven S. Gubser, Juan Martin Maldacena, Hirosi Ooguri, and Yaron Oz. Large N field theories, string theory and gravity. *Phys. Rept.*, 323:183–386, 2000.
- [3] Sean A. Hartnoll, Christopher P. Herzog, and Gary T. Horowitz. Building a Holographic Superconductor. *Phys. Rev. Lett.*, 101:031601, 2008.
- [4] Sean A. Hartnoll, Christopher P. Herzog, and Gary T. Horowitz. Holographic Superconductors. *JHEP*, 12:015, 2008.
- [5] Steven S. Gubser and Silviu S. Pufu. The Gravity dual of a p-wave superconductor. *JHEP*, 11:033, 2008.
- [6] Rong-Gen Cai, Li Li, and Li-Fang Li. A Holographic P-wave Superconductor Model. *JHEP*, 01:032, 2014.
- [7] Jiunn-Wei Chen, Ying-Jer Kao, Debaprasad Maity, Wen-Yu Wen, and Chen-Pin Yeh. Towards A Holographic Model of D-Wave Superconductors. *Phys. Rev. D*, 81:106008, 2010.
- [8] Francesco Benini, Christopher P. Herzog, Rakibur Rahman, and Amos Yarom. Gauge gravity duality for d-wave superconductors: prospects and challenges. *JHEP*, 11:137, 2010.
- [9] H. Suhl, B. T. Matthias, and L. R. Walker. Bardeen-cooper-schrieffer theory of superconductivity in the case of overlapping bands. *Phys. Rev. Lett.*, 3:552–554, Dec 1959.
- [10] Jun Kondo. Superconductivity in Transition Metals. *Progress of Theoretical Physics*, 29(1):1–9, 01 1963.
- [11] A. A. Shanenko, M. V. Milošević, F. M. Peeters, and A. V. Vagov. Extended ginzburg-landau formalism for two-band superconductors. *Phys. Rev. Lett.*, 106:047005, Jan 2011.
- [12] Mihail Silaev and Egor Babaev. Microscopic derivation of two-component ginzburg-landau model and conditions of its applicability in two-band systems. *Phys. Rev. B*, 85:134514, Apr 2012.
- [13] Pallab Basu, Jianyang He, Anindya Mukherjee, Moshe Rozali, and Hsien-Hang Shieh. Competing Holographic Orders. *JHEP*, 10:092, 2010.
- [14] Rong-Gen Cai, Li Li, Li-Fang Li, and Yong-Qiang Wang. Competition and Coexistence of Order Parameters in Holographic Multi-Band Superconductors. *JHEP*, 09:074, 2013.
- [15] Zhang-Yu Nie, Rong-Gen Cai, Xin Gao, and Hui Zeng. Competition between the s-wave and p-wave superconductivity phases in a holographic model. *JHEP*, 11:087, 2013.
- [16] Aristomenis Donos, Jerome P. Gauntlett, and Christiana Pantelidou. Competing p-wave orders. *Class. Quant. Grav.*, 31:055007, 2014.
- [17] Li-Fang Li, Rong-Gen Cai, Li Li, and Yong-Qiang Wang. Competition between s-wave order and d-wave order in holographic superconductors. *JHEP*, 08:164, 2014.
- [18] Rong-Gen Cai, Li Li, Li-Fang Li, and Run-Qiu Yang. Introduction to Holographic Superconductor Models. *Sci. China Phys. Mech. Astron.*, 58(6):060401, 2015.
- [19] Juan Martin Maldacena. Eternal black holes in anti-de Sitter. *JHEP*, 04:021, 2003.
- [20] Juan Maldacena and Leonard Susskind. Cool horizons for entangled black holes. *Fortsch. Phys.*, 61:781–811, 2013.

- [21] Rong-Gen Cai, Li Li, and Run-Qiu Yang. No Inner-Horizon Theorem for Black Holes with Charged Scalar Hairs. *JHEP*, 03:263, 2021.
- [22] Sean A. Hartnoll, Gary T. Horowitz, Jorrit Kruthoff, and Jorge E. Santos. Diving into a holographic superconductor. *SciPost Phys.*, 10(1):009, 2021.
- [23] Sean A. Hartnoll, Gary T. Horowitz, Jorrit Kruthoff, and Jorge E. Santos. Gravitational duals to the grand canonical ensemble abhor Cauchy horizons. *JHEP*, 10:102, 2020.
- [24] Yu-Sen An, Li Li, and Fu-Guo Yang. No Cauchy horizon theorem for nonlinear electrodynamic black holes with charged scalar hairs. *Phys. Rev. D*, 104(2):024040, 2021.
- [25] Yan Liu, Hong-Da Lyu, and Avinash Raju. Black hole singularities across phase transitions. *JHEP*, 10:140, 2021.
- [26] Rong-Gen Cai, Chenghu Ge, Li Li, and Run-Qiu Yang. Inside anisotropic black hole with vector hair. *JHEP*, 02:139, 2022.
- [27] Yu-Sen An, Li Li, Fu-Guo Yang, and Run-Qiu Yang. Interior structure and complexity growth rate of holographic superconductor from M-theory. *JHEP*, 08:133, 2022.
- [28] Ling-Long Gao, Yan Liu, and Hong-Da Lyu. Black hole interiors in holographic topological semimetals. *JHEP*, 03:034, 2023.
- [29] Rong-Gen Cai, Mei-Ning Duan, Li Li, and Fu-Guo Yang. Towards classifying the interior dynamics of charged black holes with scalar hair. *JHEP*, 02:169, 2024.
- [30] Rong-Gen Cai, Mei-Ning Duan, Li Li, and Fu-Guo Yang. Clarifying Kasner dynamics inside anisotropic black hole with vector hair. 8 2024.
- [31] Javier Carballo, Ayan K. Patra, and Juan F. Pedraza. Diving inside holographic metals. 8 2024.
- [32] Elena Caceres, Sanjit Shashi, and Hao-Yu Sun. Imprints of phase transitions on Kasner singularities. *Phys. Rev. D*, 109(12):126018, 2024.
- [33] Sean A. Hartnoll and Navonil Neogi. AdS black holes with a bouncing interior. *SciPost Phys.*, 14(4):074, 2023.
- [34] Elena Caceres, Arnab Kundu, Ayan K. Patra, and Sanjit Shashi. Page curves and bath deformations. *SciPost Phys. Core*, 5:033, 2022.
- [35] Yuanceng Xu, Dong Wang, and Qiyuan Pan. Page curves in holographic superconductors. *Phys. Rev. D*, 110(4):046003, 2024.
- [36] Ling-Long Gao, Yan Liu, and Hong-Da Lyu. Internal structure of hairy rotating black holes in three dimensions. *JHEP*, 01:063, 2024.
- [37] Daniel Areán, Hyun-Sik Jeong, Juan F. Pedraza, and Le-Chen Qu. Kasner interiors from analytic hairy black holes. 7 2024.
- [38] Elena Cáceres, Ángel J. Murcia, Ayan K. Patra, and Juan F. Pedraza. Kasner eons with matter: holographic excursions to the black hole singularity. 8 2024.
- [39] V. A. Belinsky, I. M. Khalatnikov, and E. M. Lifshitz. Oscillatory approach to a singular point in the relativistic cosmology. *Adv. Phys.*, 19:525–573, 1970.
- [40] Run-Qiu Yang, Rong-Gen Cai, and Li Li. Constraining the number of horizons with energy conditions. *Class. Quant. Grav.*, 39(3):035005, 2022.

- [41] Pablo Bueno, Pablo A. Cano, and Robie A. Hennigar. Kasner epochs, eras and eons. *Phys. Rev. D*, 110(4):L041503, 2024.
- [42] T. Damour, M. Henneaux, and H. Nicolai. Cosmological billiards. *Class. Quant. Grav.*, 20:R145–R200, 2003.
- [43] Marc Henneaux. The final Kasner regime inside black holes with scalar or vector hair. *JHEP*, 03:062, 2022.
- [44] Elena Caceres, Arnab Kundu, Ayan K. Patra, and Sanjit Shashi. Trans-IR flows to black hole singularities. *Phys. Rev. D*, 106(4):046005, 2022.
- [45] Alexander Frenkel, Sean A. Hartnoll, Jorrit Kruthoff, and Zhengyan D. Shi. Holographic flows from CFT to the Kasner universe. *JHEP*, 08:003, 2020.
- [46] Matan Grinberg and Juan Maldacena. Proper time to the black hole singularity from thermal one-point functions. *JHEP*, 03:131, 2021.
- [47] Justin R. David and Srijan Kumar. Thermal one point functions, large d and interior geometry of black holes. *JHEP*, 03:256, 2023.
- [48] Eivind Jørstad, Robert C. Myers, and Shan-Ming Ruan. Complexity=anything: singularity probes. *JHEP*, 07:223, 2023.